DSCC2017-5354

AN INERTIAL SENSOR TO MEASURE WIND TURBULENCE WITH RC HELICOPTERS

Anil Kumar, and Pinhas Ben-Tzvi
Robotics and Mechatronics Lab
Department of Mechanical Engineering,
Virginia Tech,
Blacksburg VA USA

ABSTRACT

This paper presents a wireless sensor system developed to use RC helicopter dynamics to measure wind turbulence. Wind turbulence is a safety concern for naval helicopter operations due to typical scarcity of landing/takeoff area on naval vessels. Wind turbulence affects the dynamics of helicopters by creating uneven thrust on the rotor blades. The proposed telemetry system, when retrofitted on an RC helicopter, extracts these external disturbances in the helicopter's dynamics and maps the wind conditions. This study focuses on learning the helicopter's dynamics in controlled wind conditions using machine learning algorithms. The presented telemetry system uses sensors such as an Inertial Measurement Unit (IMU), optical trackers, and GPS sensors to measure the dynamics of the flying RC helicopter. The system also measures the pilot's radio inputs to account for pilot inputs in the helicopter's dynamics. The telemetry system is trained and tested in a large indoor facility where turbulent wind conditions were created artificially using large wind circulation fans.

NOMENCLATURE

$\theta_0, \theta_1, \theta_2$	Collective, cyclic pitch, and cyclic roll
θ_b	Rotor blade pitch angle
η	Relative wind angle
C_A	Rotor blade lift coefficient
c	Main rotor blade airfoil chord length
ρ	Air density
U	Wind speed relative to blade element
ψ	Rotor blade position
Ω	Rotor speed
I_{xx}, I_{yy}, I_{zz}	Helicopter's moment of inertia
p, q, r	Pitch, roll and yaw rates
L, M, N	Moment along pitch, roll and yaw axis
θ, φ	Helicopter pitch and roll angles
g	Acceleration due to gravity

INTRODUCTION

Operation of rotary wing aircraft aboard ships and other sea based platforms is a very risky and challenging task. The situation becomes even more complicated when the surrounding air interacts with the cruising ship's superstructure to leave behind a trail of wind disturbance (involving both steady state and turbulent wind flow), or ship air wakes. These ship air wakes interacting with helicopters operating in close vicinity to the ships can result in unwanted oscillations, which, when combined with limited landing deck area, pose serious safety concerns. To mitigate these operational risks, 'safe launch and recovery envelopes' are prescribed for each class of naval vessels in order to avoid high air wake zones [1]. To determine these safe launch and recovery envelops, Computational Fluid Dynamics (CFD) models are used. Significant research has been done to develop high fidelity CFD models in order to study the interaction of wind with moving ship's superstructure and then to predict air wake patterns [2,3]. However, validation and refinement of such CFD models require extensive experimental data. To obtain experimental ship air wake data for the validation of CFD models, the most commonly used methods are wind tunnel testing and in-situ wind measurements using anemometers.

Wind tunnel testing is the most popular tool for experimentally validating wind-solid body interactions in the aerospace science community. During testing, scaled down model of test bodies (vessels) are made to interact with controlled streamlined wind flow (to match Reynold's number) and the resulting turbulent wind pattern is measured. Such wind tunnel setups utilize a variety of anemometric modalities including laser sensing [4], hot wire anemometers [2,5] and

Particle Image Velocimetry [6,7]. Although the transducers used in the wind tunnels are extremely sensitive, due to very high cost they cannot be deployed outside the limited test area of a wind tunnel. Furthermore, wind tunnels cannot generate fine details of flow patterns because of the losses in structural details due to the scaling of the test model. Additionally, errors in flow pattern arising from the model holder and wind tunnel parts must be accounted for in the measurements.

Use of outdoor anemometers is another common means for in-situ wind pattern measurement. Multiple ultrasonic anemometers are placed at different locations on the flight deck of the naval vessels and the measurements are compared with CFD/Wind Tunnel testing results [2,4,8,9]. In this methodology, the high cost of the anemometers limits the number of anemometers used simultaneously, whereas moving the sensors to different positions is time consuming. To overcome this limitation, Mallon et al. [10] in a similar study used airborne anemometers mounted on a quadrotor to map ship air wakes. This requires compensation of the UAV's own wakes and motion relative to the inertial frame of reference.

To overcome these limitations Kumar et al. have proposed the use of RC helicopters with machine learning algorithms to extract ship air wake patterns [11–15]. Air wakes aerodynamically affect RC helicopters the same way they do to full-scale helicopters. Therefore, helicopter dynamics can be mapped to wind conditions. Whereas previous work was focused on modelling helicopter's response to pilot inputs in absence of wind turbulence, this paper models the same in a controlled wind environment. This paper presents a study on modeling the helicopter's dynamics in different wind conditions using neural networks and then using the same model to estimate wind conditions.

BACKGROUND

Helicopters are rotary wing aircraft, which use thrust vectoring for attitude control and maneuvering. A swash plate mechanism in the rotor hub plays a pivotal role in the helicopter's control by transferring actuator inputs from the stationary (not-rotating) helicopter fuselage to the rotating blades [16]. The swash plate makes rotor pitch angle a function of rotor position. The pilot inputs received by the helicopter's main rotor consist of three components: roll cyclic, pitch cyclic, and collective. The roll and pitch cyclic inputs result in a differential rotor pitch angle, which helps the helicopter to tilt and maneuver by creating differential thrust along the pitch and roll axes. Collective inputs on the other hand, result in uniform lift-off thrust throughout the rotor disk area by contributing to offset the rotor pitch value.

Modelling the helicopter as a 3D rigid body, the Newton-Euler equations for the rotational motion of the helicopter can be represented as follows:

$$
\begin{aligned}
I_{xx}\dot{p} &= qr\left(I_{yy} - I_{zz}\right) + \left(L_{mr} + L_g\right) \\
I_{yy}\dot{q} &= rp\left(I_{zz} - I_{xx}\right) + \left(M_{mr} + M_g\right) \\
I_{zz}\dot{r} &= pq\left(I_{xx} - I_{yy}\right) + \left(-N_{mr} + N_{tr}\right)
\end{aligned}
\tag{1}
$$

Here subscripts mr and g represent 'main rotor' and 'gravity' respectively. Fig. 1A shows the frame of reference assignment for the helicopter. The gravity component in the helicopter's rotation dynamics is a result of the fact that the center of mass and the center of rotation of the helicopter are not the same. This results in a pendulum-type restoring moment (Fig. 1C, 1D) whenever the aerodynamic loading on the rotor blades tilt the helicopter. The main rotor moment is primarily composed of two components: pilot inputs and wind conditions [16,17]. If the helicopter's main rotor blade is assumed to be composed of infinitesimally thin airfoil elements (of thickness dr_b), then the differential liftoff (dl) generated by each element can be computed as follows:

$$
dl(\psi) = \tfrac{1}{2}\rho U^2 C_A c\left(\theta_b(\psi) - \eta\right) dr_b
\tag{2}
$$
$$
\theta_b(\psi) = \theta_0 + \theta_1 \cos(\psi) + \theta_2 \sin(\psi); \quad \eta = \tan^{-1}\frac{U_n}{U_t}
$$

Here U_n and U_t are the normal and tangential components of the wind (U) relative to the moving rotor blade air foil in the rotor plane. From (2) it is clear that the thrust generated by the rotor blades depends on both the wind direction (η) and pilot inputs (θ_b).
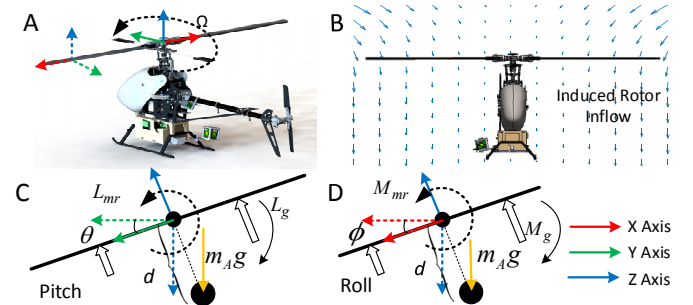
Figure 1. Helicopter dynamics: (A) Frame of reference assignment, (B) Induced rotor inflow, (C) Helicopter pitch dynamics and (D) Helicopter roll dynamics.

Because of mechanical constraints in the swash plate, it is straightforward to model the rotor pitch angle; however modelling the wind angle is very difficult due to unpredictable wind flow in turbulent environments. The wind angle relative to the rotor blades is thus extracted from steady state flow conditions. The steady state external wind flow is modelled using a 12-parameter linear model as shown below:

$$
\begin{bmatrix} u_x \\ u_y \\ u_z \end{bmatrix}_{wh}
=
\begin{bmatrix} a_x & b_x & c_x \\ a_y & b_y & c_y \\ a_z & b_z & c_z \end{bmatrix}
\begin{bmatrix} x \\ y \\ z \end{bmatrix}
+
\begin{bmatrix} d_x \\ d_y \\ d_z \end{bmatrix};
\quad
\begin{bmatrix} x \\ y \\ z \end{bmatrix}
=
\begin{bmatrix} r_b c\psi \\ r_b s\psi \\ 0 \end{bmatrix}
\tag{3}
$$

Here $s\psi$ and $c\psi$ represent sine and cosine of the rotor position angle. If the rotor blade airfoil section under consideration is at a radial distance r_b from the rotor hub assembly, then the wind relative to the airfoil due to its motion

is $[0\ \Omega r_b\ 0]^T$ and using this information, it is possible to estimate the wind relative to the blade. Here, effects of rotor flapping are ignored and it is assumed that the main rotor blades rotate in a fixed plane with respect to the helicopter's fuselage.

$$\begin{bmatrix} u_x \\ u_y \\ u_z \end{bmatrix}_{wb} = R_b^h \left(\begin{bmatrix} u_x \\ u_y \\ u_z \end{bmatrix}_{wh} - \begin{bmatrix} 0 \\ 0 \\ v \end{bmatrix}_{ih} - \begin{bmatrix} u_x \\ u_y \\ u_z \end{bmatrix}_{bh} \right) ; \begin{bmatrix} u_x \\ u_y \\ u_z \end{bmatrix}_{bh} = \begin{bmatrix} 0 \\ \Omega r_b \\ 0 \end{bmatrix} \quad (4)$$

By using equations (2) and (4), the wind inclination angle can be computed as follows:

$$\eta \approx \frac{d_z + a_z r_b\, c\psi + b_z r_b\, s\psi - v_{ih}}{-\Omega r_b + c\psi\left(d_y + a_y r_b\, c\psi + b_y r_b\, s\psi\right) - s\psi\left(d_x + a_x r_b\, c\psi + b_x r_b\, s\psi\right)} \quad (5)$$

Here, v_{ih} is the induced rotor inflow, which is assumed to be constant for near-hover flight conditions. As the rotor speed term in the denominator is much larger than the remaining terms, the wind inclination angle (η) is proportional to a_z and b_z, coefficients of the wind model which represent vorticity in pitch and roll axis respectively in the rotor plane. With η being proportional to rotor blade liftoff (2), it is also proportional to the main rotor moment along the roll and pitch axis (1) [17].
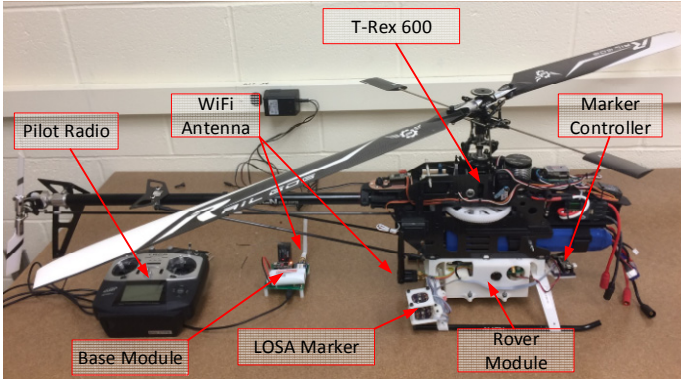

Figure 2. Sensing system hardware setup.

SYSTEM HARDWARE SETUP

The proposed sensor system consists of two custom-made instrumentation modules, referred to as the rover module and the base module (Fig. 2). The rover module is retrofitted onto a T-Rex 600 series RC helicopter, and primarily consists of an aviation grade INS/IMU (VN200) sensor. The base module communicates with the rover module over a low latency Wi-Fi network to receive the helicopter's dynamics wirelessly. The base module is also equipped with an RC receiver to receive pilot input and then relay the pilot inputs along with the helicopter dynamics to a PC for processing and recording over a USB link. In addition to the helicopter's dynamics, the helicopter's position is equally important.

The proposed system uses the Linear Optical Sensor Array based tracking system [18] for tracking the helicopter's spatial

motion in an indoor environment. A cubical shaped active marker was retrofitted onto the helicopter (as shown in Fig. 2) to measure the helicopter's position, linear velocity, and attitude relative to a stationary tracking device during the experiments. The system was able to acquire helicopter dynamics at an average update rate of 140 Hz and position estimates from the LOSA tracker at 320 Hz. Fig. 3 shows the electrical schematics of the rover and the base module.
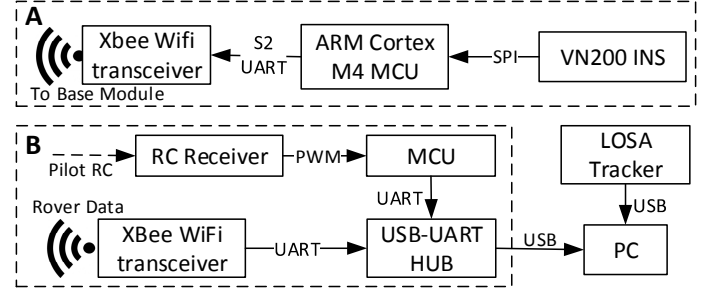

Figure 3. Electrical schematics of: (A) Rover module, and (B) Base module.

To obtain a controlled wind dataset for training the system, a wind mapping platform was created. The wind mapping setup used two 24-inch diameter wind circulation fans to create an artificial wind flow (Fig. 4A). The system used a Young® 81000 3-axis ultrasonic anemometer mounted on a pole (with caster wheeled base) as the primary sensor [19]. The anemometer was interfaced with using an ARM® Cortex M4 microcontroller through analog inputs. The micro controller also hosted a 9-axis IMU with AHRS implementation. The attitude-corrected wind flow measurements were sent to a PC for recording over a Wi-Fi network. The anemometer was also retrofitted with a LOSA marker for tracking the motion of the anemometer with respect to the already stationary LOSA tracker (Fig. 4B, 4C). The anemometer readings were compensated for its motion and converted in the tracker's frame of reference.
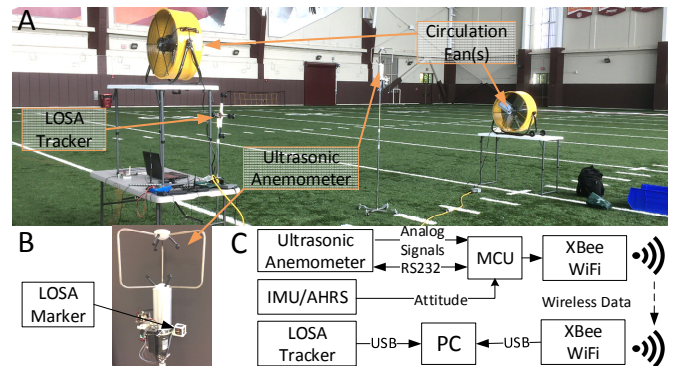

Figure 4. (A) Wind mapping setup[17]; (B) Ultrasonic anemometer, (C) Electrical schematics.

INDOOR EXPERIMENTATION

To test the capability of the telemetry system, the helicopter was flown in a wind controlled indoor environment. To generate artificial wind conditions, a setup of two air circulation fans placed opposite to each other was implemented (shown in Fig. 4A).

To map the wind flow, the anemometer was moved between the two fans at different heights and the wind flow was measured, along with the position and velocity of the anemometer. The recorded data was then interpolated using bilinear interpolation to a grid of size 5cm to obtain the steady state flow field as shown in Fig. 5.
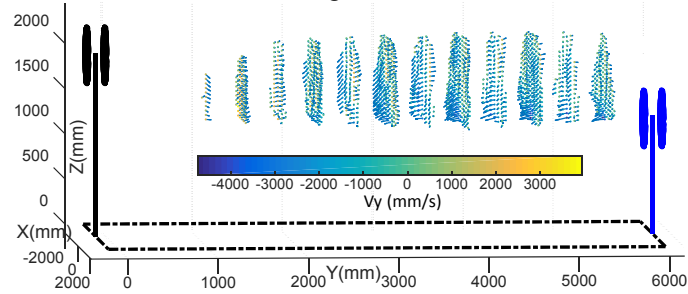
Figure 5. Measured steady state flow field.

In addition to the steady state flow, the standard deviation of the wind speed (over a duration window of 2s) was also computed to characterize wind turbulence in the region of interest. Fig. 6 shows the distribution of the standard deviation of the wind speed (in the form of slice plot) for the flow field shown in Fig. 5. The average value of turbulence (std. deviation of wind speed) was estimated to be 28 mm/s.
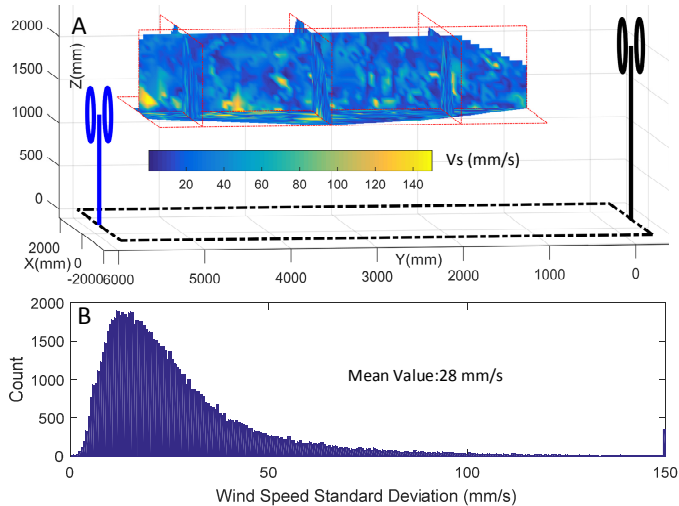

Figure 6. Measured wind turbulence: (A) Spatial Distribution, (B) Distribution histogram for Wind Speed

The wind map setup created with the two fan setup provided ground truth for the wind-flow conditions to be tested with the proposed instrumentation system. The RC helicopter mounted with the rover module and LOSA marker was flown

in the test volume and quantities like angular acceleration, angular rates, pilot inputs, and attitude (angles) were recorded.

SYSTEM TRAINING AND RESULTS

As shown in the previous section, the wind conditions affect the helicopter's dynamic response to pilot input. Therefore, if the helicopter's dynamic model with state variables is known, it is possible to extract wind conditions from the helicopter's dynamics measurements. The proposed system uses Back Propagation Neural Network (BPNN) [20] to find the mapping between the helicopter dynamics variables and wind condition. As suggested in (1), angular acceleration measurements of the helicopter depend on pilot inputs, wind conditions, angular rate measurement, and tilting angle (roll and pitch). Thus, the proposed system uses two BNNNs to predict wind vorticity (Roll/Pitch) from eight-dimensional input vectors consisting of three swash plate pilot inputs, three channel angular rates, the measured angular acceleration (Roll/Pitch) and the tilting angle (Roll/Pitch). For training and testing of the networks, the wind vorticity of the steady state flow field was obtained by fitting the data on the linear model shown in (3). The estimated wind vorticities in the inertial (LOSA tracker's) frame of reference were converted into the helicopter's frame of reference based on attitude estimates obtained from the LOSA tracker and fed to the neural network.
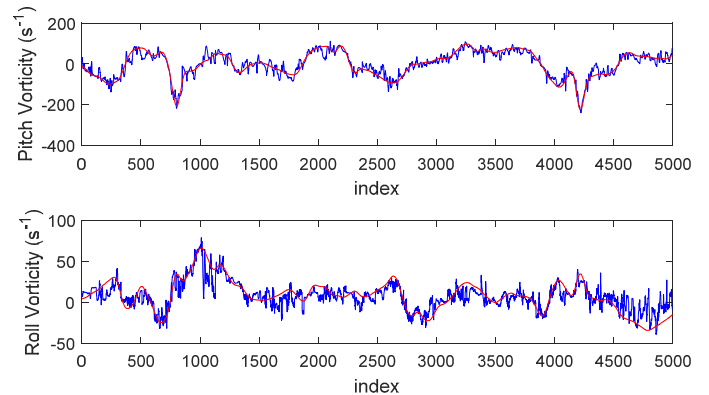

Figure 7: Neural Network prediction results (blue) with measured estimates (red) for wind vorticity.

To model the helicopter's nonlinear dynamics, 2-hidden layered BPNNs were trained. The BP Neural network topology was selected through trial and error. The system was trained with the number of neurons in hidden layers varied from 4 to 15. It was observed that the neural networks with hidden layer topology {8, 6} and {10, 5} deliver the best prediction accuracy. To prevent overtraining of the system, 10-fold cross validation [21] was used with the back propagation training algorithm. The networks were trained using around 7100 data samples and tested on around 15000 samples. Fig. 7 shows the prediction results for the two neural networks predicting ambient wind vorticity on a subset of the test database. Fig. 8 shows the histogram plot from the distribution of the absolute prediction error in wind vorticities.
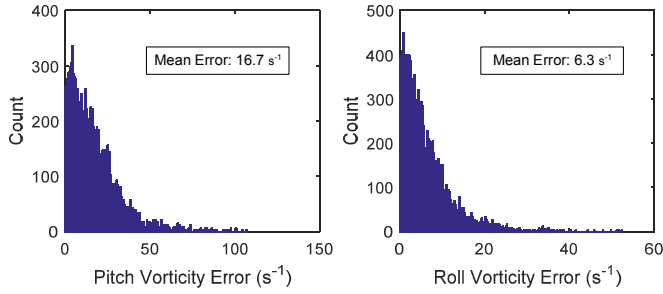
Figure 8. Neural Network output error Distribution.

The trained networks were also tested by comparing generated wind vorticity patterns with measured steady state vorticity. Fig. 9 shows qualitative comparison between the predicted vorticity pattern and the measured vorticity pattern in the form of 3D slice plots. High correlation is visible in wind vorticity distribution in the Z-Y plane (right column).
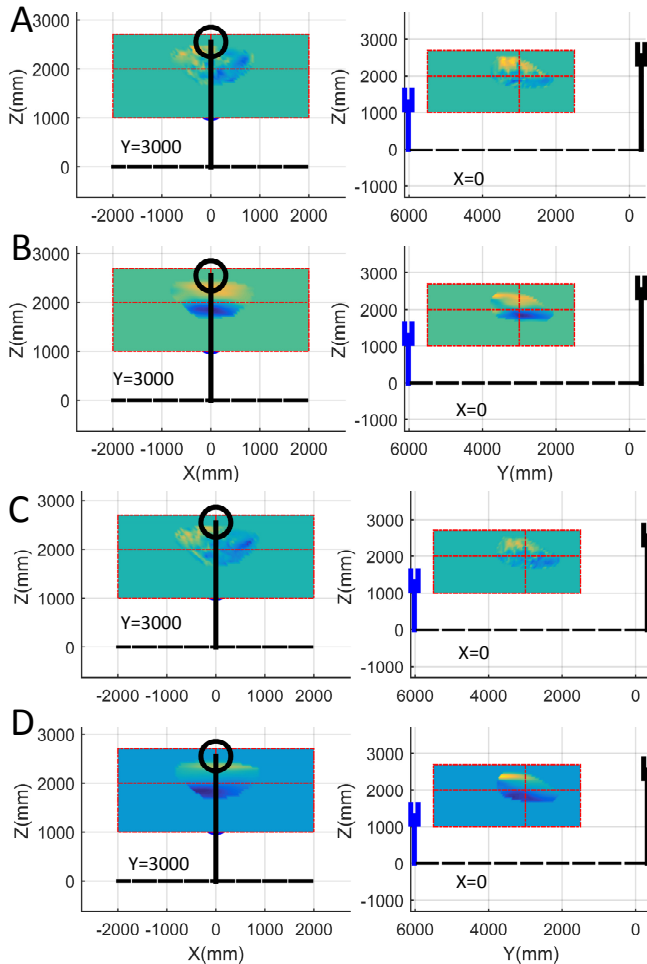
Figure 9. Wind vorticity patterns: (A) Predicted Vorticity along x axis, (B) Measured Vorticity along x axis, (C) Predicted Vorticity along y axis, (D) Measured Vorticity along z axis.

CONCLUSIONS

This paper presented a novel study using helicopter dynamics for sensing and mapping wind flow patterns in an indoor environment. The system was able to estimate artificially created turbulence patterns during indoor experiments with fair accuracy. The presented system removes rotor blade dynamics in the helicopter's angular acceleration data by using a low pass filter which distorts the low frequency dynamics. The authors plan to add a rotor blade tracking sensor to the system which then can be used to estimate rotor position and dynamics, and will significantly improve the accuracy of the system.

System limitations: The system currently relies on the rotational impact of wind turbulence and hence can only estimate the vorticity aspect of air wakes. By including the helicopter's linear drift in the system model, the laminar flow component of the wind pattern can also be estimated using the proposed system. The system also assumes steady state flow conditions during training and testing of the system, but turbulence is present in the system as shown in Fig. 6. This turbulence is a major source of prediction error in the neural networks.

ACKNOWLEDGMENTS

REFERENCES

[1]   NAVAIR, 2003, *Helicopter Operating Procedures for Air-Capable Ships NATOPS Manual*.

[2]   Snyder, M. R., Kang, H. S., Brownell, C. J., Luznik, L., Miklosovic, D. S., Burks, J. S., and Wilkinson, C. H., 2011, "USNA Ship Air Wake Program Overview," *29th AIAA Applied Aerodynamics Conference*, Honolulu, Hawaii, pp. 1–12.

[3]   Polsky, S., Imber, R., Czerwiec, R., and Ghee, T., 2007, "A Computational and Experimental Determination of the Air Flow Around the Landing Deck of a US Navy Destroyer (DDG): Part II," *37th AIAA Fluid Dynamics Conference and Exhibit*, Miami, Florida, pp. 1–12.

[4]   Bardera-Mora, R., Barcala-Montejano, M. A., Rodríguez-Sevillano, A., de Diego, G. G., and de Sotto, M. R., 2015, "A Spectral Analysis of Laser Doppler Anemometry Turbulent Flow Measurements in a Ship Air Wake," *Proc. Inst. Mech. Eng. Part G J. Aerosp. Eng.*, pp. 1–12.

[5]   Roper, D. M., Owen, I., Padfield, G. D., and Hodge, S. J., 2006, "Integrating CFD and Piloted Simulation to Quantify Ship-Helicopter Operating Limits," Aeronaut. J., **110**(1109), pp. 419–428.

[6]   Silva, M. J., Wadcock, A. J., Yamauchi, G. K., and

Long, K. R., 2004, "Wind Tunnel Investigation Of The Aerodynamic Interactions Between Helicopters And Tiltrotors In A Shipboard Environment," *American Helicopter Society 4th Decennial Specialist's Conference on Aeromechanics*.

[7] Wadcock, A. J., Yamauchi, G. K., Heineck, J. T., Silva, M. J., and Long, K. R., 2004, "PIV Measurements of the Wake of a Tandem-Rotor Helicopter in Proximity to a Ship," Am. Helicopter Soc. Aeromechanics Spec. Forum, pp. 1–23.

[8] Snyder, M. R., Kang, H. S., Brownell, C. J., and Burks, J. S., 2012, "Validation of Ship Air Wake Simulations and Investigation of Ship Air Wake Impact on Rotary Wing Aircraft," Am. Soc. Nav. Eng. Launch Recover. Symp., p. 18.

[9] Snyder, M. R., Kang, H. S., and Burks, J. S., 2012, "Comparison of Experimental and Computational Ship Air Wakes for a Naval Research Vessel," *Proc. 30th AIAA Applied Aerodynamics Conf.*, pp. 1–25.

[10] Mallon, C. J., Muthig, B. J., Gamagedara, K., Patil, K., Friedman, C., Lee, T., and Snyder, M. R., 2017, "Measurements of Ship Air Wake Using Airborne Anemometers," *55th AIAA Aerospace Sciences Meeting*, pp. 1–12.

[11] Kumar, A., Ben-Tzvi, P., Saab, W., and Snyder, M. R., 2016, "Wireless Telemetry System for Real-Time Estimation of Ship Air Wakes with UAVs," Mechatronics, **36**, pp. 18–26.

[12] Kumar, A., Ben-Tzvi, P., and Snyder, M. R., 2015, "UAV-Based Wireless Telemetry System for the Estimation of Ship Air Wake Patterns," *ASME International Design Engineering Technical Conference & Computers and Information in Engineering Conference*, Boston, Massachusetts, USA, pp. 1–7.

[13] Kumar, A., and Ben-tzvi, P., 2016, "Extraction of Impact of Wind Turbulence on RC Helicopters Using Machine Learning," *ASME International Design Engineering Technical Conference*, Charlotte, North Carolina, pp. 1–7.

[14] Snyder, M. R., Kumar, A., and Ben-Tzvi, P., 2014, "Off Ship Measurement of Ship Air Wakes Using Instrumented Unmanned Aerial Vehicles," *AIAA Applied Aerodynamics Conference*, pp. 1–9.

[15] Kumar, A., Ben-Tzvi, P., Snyder, M. R., and Saab, W., 2013, "Instrumentation System for Ship Air Wake Measurement," *ROSE 2013 - 2013 IEEE International Symposium on Robotic and Sensors Environments, Proceedings*, pp. 118–123.

[16] Padfield, G. D., 2007, *Helicopter Flight Dynamics: The Theory and Application of Flying Qualities and Simulation Modelling*, Blackwell Publishing, Oxford UK.

[17] Kumar, A., and Ben-Tzvi, P., 2017, "Novel Wireless Sensing Platform for Experimental Mapping and Validation of Ship Air Wake," IEEE/ASME Trans. Mechatronics, Under Rev.

[18] Kumar, A., and Ben-Tzvi, P., 2016, "Spatial Object Tracking System Based on Linear Optical Sensor Arrays," IEEE Sens. J., **16**(22), pp. 7933–7940.

[19] "R. M. Young Company Ultrasonic Anemometer - Model 81000" [Online]. Available: http://www.youngusa.com/products/6/3.html. [Accessed: 16-Sep-2016].

[20] Bishop, C. M., 2006, *Pattern Recognition and Machine Learning*, Springer-Verlag New York.

[21] Kohavi, R., 1995, "A Study of Cross-Validation and Bootstrap for Accuracy Estimation and Model Selection," *International Joint Conference on Artificial Intelligence*, pp. 1137–1143.